iScience

CellPress
OPEN ACCESS

Article

Electron Transport Chain Complex II Regulates Steroid Metabolism

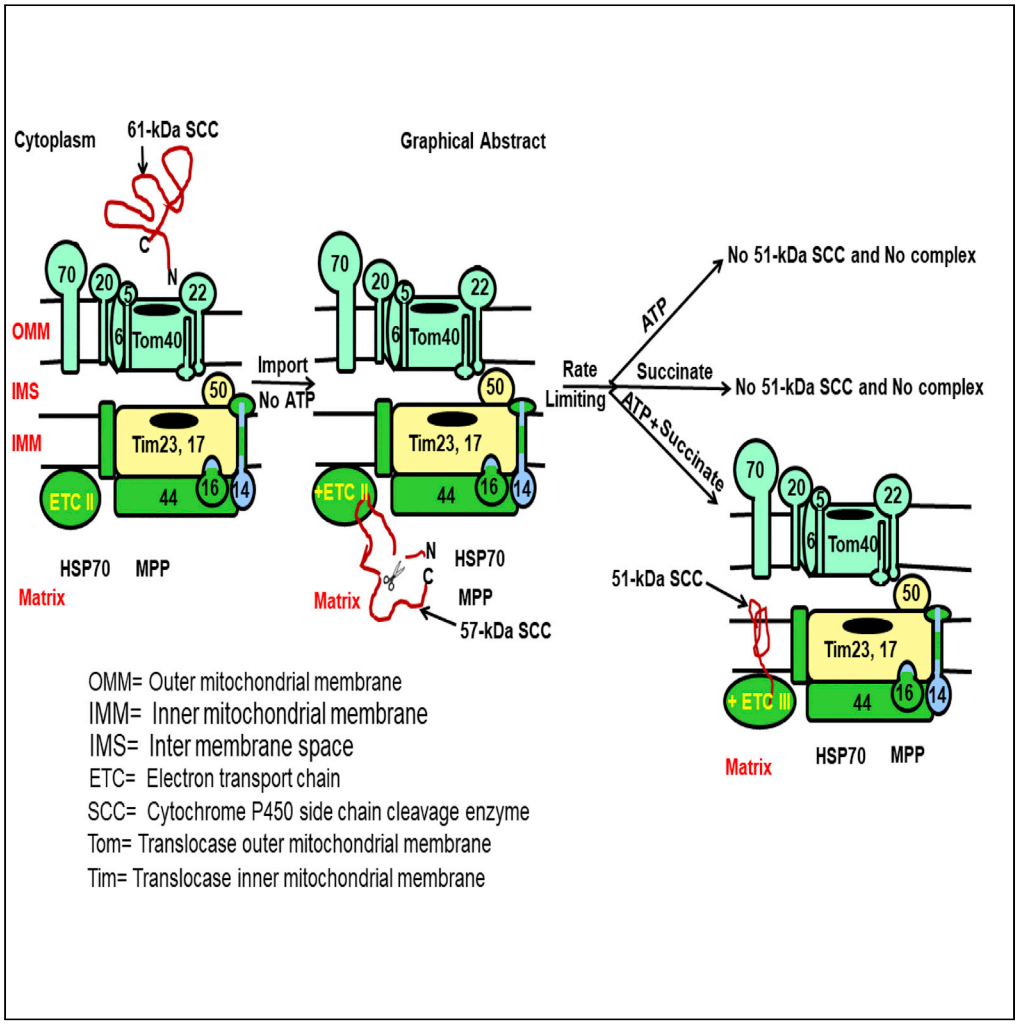

Himangshu S. Bose, Brendan Marshall, Dilip K. Debnath, Elizabeth W. Perry, Randy M. Whittal

bose_hs@mercer.edu

HIGHLIGHTS

P450 SCC synthesizes first steroid with the electrons from ETC complex III to IV

Succinate from complex II activates complex III for the metabolic activity

Absence of succinate ablates mitochondrial processing of SCC and metabolic activity

Succinate anion stabilizes ETC complex II for the activation of steroid metabolism

Bose et al., iScience *23*, 101295
July 24, 2020
https://doi.org/10.1016/j.isci.2020.101295

iScience

CellPress
OPEN ACCESS

Article

Electron Transport Chain Complex II Regulates Steroid Metabolism

Himangshu S. Bose,[1,4,6,*] Brendan Marshall,[2] Dilip K. Debnath,[1,5] Elizabeth W. Perry,[2] and Randy M. Whittal[3]

SUMMARY

The first steroidogenic enzyme, cytochrome P450-side-chain-cleavage (SCC), requires electron transport chain (ETC) complexes III and IV to initiate steroid metabolic processes for mammalian survival. ETC complex II, containing succinate dehydrogenase (quinone), acts with the TCA cycle and has no proton pumping capacity. We show that complex II is required for SCC activation through the proton pump, generating an intermediate state for addition of phosphate by succinate. Phosphate anions in the presence of succinate form a stable mitochondrial complex with higher enthalpy (-ΔH) and enhanced activity. Inhibition of succinate action prevents SCC processing at the intermediate state and ablates activity and mitochondrial protein network. This is the first report directly showing that a protein intermediate state is activated by succinate, facilitating the ETC complex II to interact with complexes III and IV for continued mitochondrial metabolic process, suggesting complex II is essential for steroid metabolism regulation.

INTRODUCTION

Mitochondria are critical for many activities, including bioenergetics, biosynthesis, and signaling. Diseases associated with mitochondrial errors in metabolism are the most common of inherited metabolic disorders (Vafai and Mootha, 2012) given that steroid hormone synthesis is initiated in the mitochondria of specific cells (Figure 1A). Mitochondrial stress responses triggered by a primary molecular defect are the major contributing factor to different mitochondrial metabolic disorders (Suomalainen and Battersby, 2017). To combat these deleterious outcomes and maintain mitochondrial function and integrity, cells use a network of mitochondrial protein-protein interactions, including those that precede integration of proteins during translocation and into mitochondria (Itakura et al., 2016).

Steroid hormones have potent physiological effects; most are made in the adrenals and gonads (ovaries for women), but the brain also synthesizes steroids (Miller and Auchus, 2011). Steroid synthesis is initiated when the side chain of cholesterol is cleaved by the cytochrome P450 side chain cleavage enzyme (P450scc or SCC) (Chung et al., 1986) in association with six electrons from NADPH-ferredoxin and ferredoxin reductase of the electron transport chain (ETC) complex III and IV, thereby catalyzing cholesterol to pregnenolone (Figure 1A). A build-up of uncatalyzed cholesterol would engorge the cells, destroying metabolic activity and deforming organelle structure (Bose et al., 1996). SCC inactivity is incompatible with full-term gestation, and a partial SCC defect results in pseudo-hermaphroditism in genetic males and lack of secondary sexual characteristics in genetic females (Kaur et al., 2016; Miller and Auchus, 2011). In addition, polymorphisms in the SCC locus are linked to polycystic ovary syndrome (Shan et al., 2016), one of the most common increasing reproductive disorders around the world (Ding et al., 2017).

SCC is a member of the type 1 mitochondrial P450 family of enzymes, requiring ETC complex III, IV, or V (Miller, 2017a). ETC complex II or succinate dehydrogenase (quinone) is shared with the tricarboxylic acid cycle (TCA) cycle; it has no proton pumping capacity and was not known to have any role in steroid metabolism. Succinate, an intermediate metabolite in the TCA cycle (Matsumoto et al., 2012), is generated from succinyl-CoA in the TCA cycle and has a hormone-like function (Guo et al., 2017; He et al., 2004). SCC is expressed as a precursor 61-kDa protein and following mitochondrial import forms an intermediate 57-kDa and mature 51-kDa protein (Bose et al., 2019). SCC requires NADPH, Ferredoxin, and Ferredoxin reductase in complex III (Miller, 2017b) at the inter mitochondrial membrane (IMM). Here, we show that the ETC complex II requires complex III for activation, where the proton pump facilitates the formation of an active SCC folding in the intermediate state at the matrix. In the presence of ATP, succinate anions

[1]Biomedical Sciences, Mercer U School of Medicine, Memorial University Medical Center, 1250 East 66th Street, Savannah, GA 31404, USA

[2]Department of Cellular Biology and Anatomy, Augusta University, Augusta, GA, USA

[3]Department of Chemistry, University of Alberta, Edmonton, Canada

[4]Anderson Cancer Institute, Savannah, GA, USA

[5]Present address: Department of Chemistry, Coochbehar Panchanan Burma University, Coochbehar, West Bengal, India

[6]Lead Contact

*Correspondence: bose_hs@mercer.edu

https://doi.org/10.1016/j.isci.2020.101295

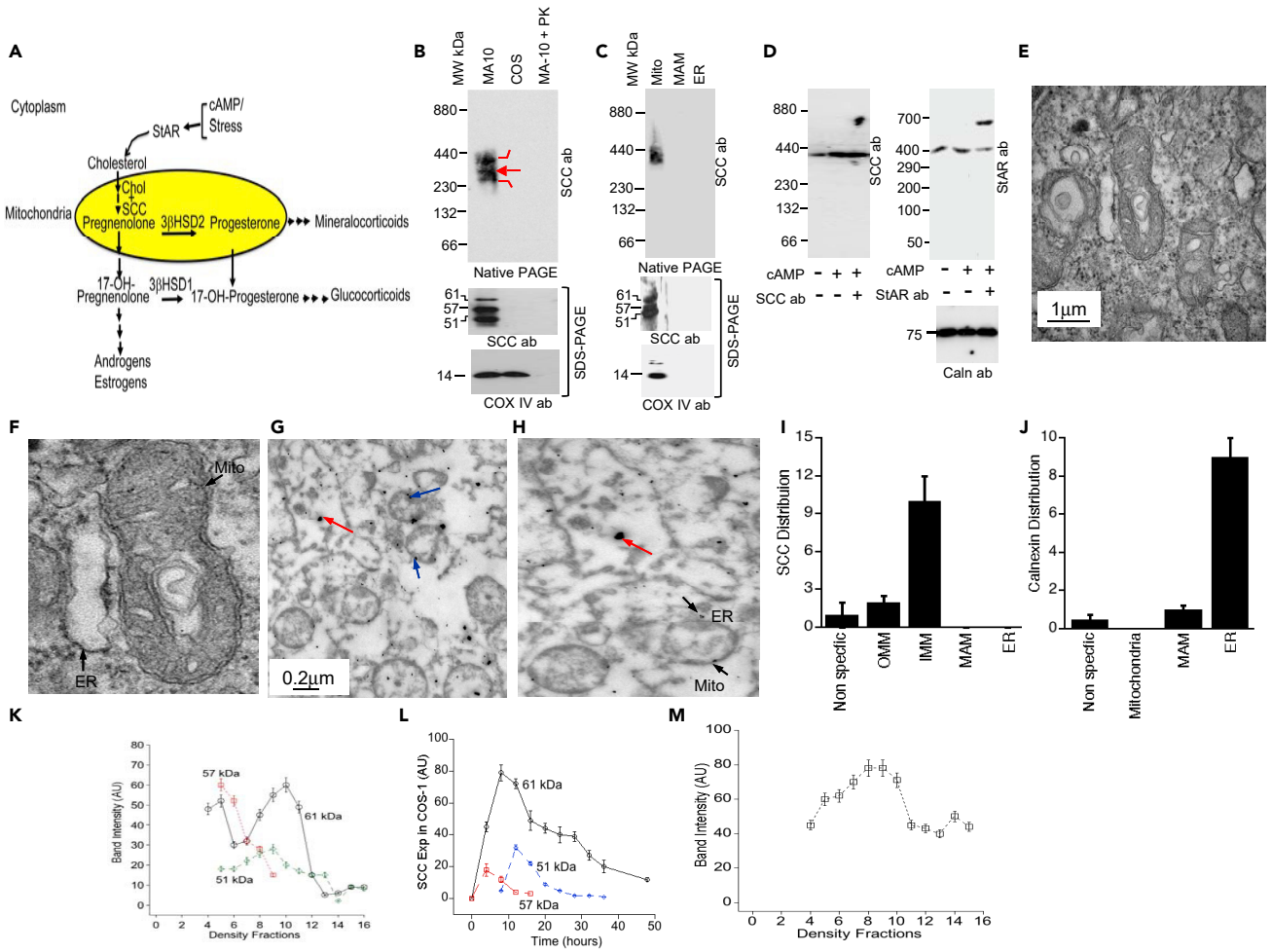

Figure 1. SCC Localization and Mitochondrial Import

(A) Simplified schematic presentation of the first step of steroidogenesis, where cholesterol is catalyzed to pregnenolone by the P450 side chain cleavage enzyme (SCC).

(B) (Top) Native gradient page analysis of the digitonin-solubilized complex from MA-10 and COS-1 cells. Western blotting with SCC antibody. Middle and bottom, SDS-PAGE western blotting with SCC (middle) and COX-IV antibodies independently (bottom).

(C) (Top) Analysis of the digitonin-solubilized complex of mitochondria, MAM, and ER through 6%–16% native gradient PAGE and visualized by western blotting with SCC antibody. (Middle) Analysis of the same fractions through SDS-PAGE and western blotting with SCC antibody. (Bottom) Western blotting of the same fractions in the middle panel with COX-IV antibody.

(D) (Left) Antibody shift experiment after stimulation of MA-10 cells with cAMP of the digitonin lysate with SCC antibody followed by analysis through a native gradient PAGE and western blotting with SCC antibody. (Right) Antibody shift of the same digitonin lysate with StAR antibody analyzed through native gradient page and western blotting with StAR antibody. (Bottom) SDS-PAGE analysis of the digitonin fractions followed by western blotting with a calnexin antibody.

(E) EM analysis of mouse testis in absence of any antibody.

(F) Enlarged mitochondrion from (E). ER and mitochondria (mito) are indicated with a black arrow.

(G) Immuno-EM of testicular cells stained with SCC (blue arrowheads) and calnexin (red arrow) antibodies together.

(H) An enlarged view of the ER and mitochondria from (G).

(I and J) Quantitative analysis of the distribution of SCC (G) and calnexin (H) in testicular cells.

(K) Quantitative analysis of the processing of 61-kDa (black solid line with ○), 57-kDa (blue broken line with ◇), and 51-kDa (red half dotted line with □) SCC after overexpression in COS-1 cells at the indicated time and identified by western blotting with an SCC antibody.

(L) Quantitative analysis of density gradient fractions from mouse testes and western blotting with SCC antibody. The distribution pattern of the 61-kDa (solid black line, -O-), 57-kDa (dotted red line, square), and 51-kDa (green half-broken line, -O-) SCC.

(M) Analysis of the density distribution fractions from (L). Western blotting with VDAC2 antibody. (I) and (J) are means ± SEM from three independent experiments performed three times.

See also Figures S1 and S2 and Table S1.

generate the final, folded, active state of 51-kDa SCC, which is dependent on the availability of the 57-kDa protein. SCC metabolic activity reaches a maximum level with the lowest heat content (enthalpy), generating the most stable state. For the first time, we show that, at the mitochondrial matrix, SCC processing is the rate-limiting state, which is activated by succinate and facilitates ETC complex II interaction with complexes III and IV for cellular metabolism.

RESULTS

Transport of SCC to the Matrix

Following synthesis by membrane-free ribosomes, mitochondrial targeting SCC may be folded at the mitochondria-associated-ER membrane (MAM) (Prasad et al., 2017) prior to loading at the OMM or directly passing to the IMS or matrix. To understand the processing mechanism of SCC, we prepared digitonin lysate of mouse testes, analyzed in a native gradient PAGE and western blotted with the SCC antibody. The results show three closely associated complexes (Figure 1B), but mass spectrometric analysis identified the presence of identical proteins in each (Table S1), suggesting that the smaller complexes are due to breakdown of the major complex or that during translocation SCC possibly proceeds through different steps of folding while being associated with the same network of proteins. We did not find any complex with nonsteroidogenic COS-1 cells, suggesting specificity of SCC-associated complex proteins. To further examine SCC translocation from the endoplasmic reticulum (ER) to the mitochondrial matrix, we isolated mitochondria and cytoplasm from mice testes; solubilized the ER, mitochondria, and MAM fractions in digitonin; and separated them through a native gradient PAGE followed by western blotting with SCC antibody. The 400-kDa SCC complex was detected in the mitochondrial fraction and completely absent in the MAM (mitochondria-associated ER membrane) (Hayaski et al., 2009) and ER fractions (Figure 1C). Western blotting of the complex analyzed through SDS-PAGE confirmed the presence of SCC in the mitochondrial fraction with 61-, 57-, and 51-kDa fragments (Figure 1C, middle panel). Matrix resident COX IV was present in the mitochondrial fraction, indicating the accuracy of complex purification. An antibody shift with SCC antibody in digitonin-solubilized cytoplasmic fraction of the cAMP-stimulated mouse Leydig (MA-10) cells did not show any high-molecular-weight complex (Figure 1D, left panel) but showed a molecular weight shift with the StAR antibody (Prasad et al., 2017) (Figure 1D, right panel), suggesting that SCC does not require chaperone or cytoplasmic proteins for folding prior to loading onto the mitochondrial membrane and may be directly imported into mitochondria.

If SCC is imported directly into mitochondria, we hypothesized that it may have limited residency at the OMM. We directly visualized SCC subcellular localization through immunoelectron microscopy in the mouse testis. The organelle structure is protected (Figure 1E) with clear outer and inner mitochondrial membranes (Figure 1F). The ER is in close proximity to mitochondria (Figure 1G and its enlarged version in Figure 1H) with distances of 0.29, 0.09, and 0.05 μm (Figure S1, enlarged version), suggesting that mitochondria at 0.09 and 0.05 μm are likely to form the MAM, which may be ideal for direct loading onto the OMM. Semi-quantitative analysis of SCC localization in testicular cells showed that the majority remained at the IMM (9.87 $\pm$ 2.1 per 81μm^2 field of view) and a small amount remained at the OMM (2.0 $\pm$ 0.5 per 81μm^2 field of view) (Figure 1G, blue arrow, 15-nm gold particle size and Figure 1I), suggesting that SCC was processed directly into mitochondria. As expected, calnexin was found predominantly in the ER (9.1 $\pm$ 1.0 per 81μm^2 field of view) with a small number found in the MAM fraction (0.95 $\pm$ 0.11 per 81μm^2 field of view) (Figure 1G, red arrow in 55-nm gold particle size and Figure 1J), indicating the accuracy of localization.

SCC Folding States Are Kinetically Controlled

Acute steroid regulation is rapid but not instant, suggesting that SCC requires appropriate folding after mitochondrial entry to initiate catalysis of substrate cholesterol. We studied mitochondrial processing kinetics after expression in nonsteroidogenic COS-1 cells and measured expression by western blotting with SCC antibody. Nonsteroidogenic cells were selected to avoid endogenous SCC expression. As shown in Figure 1K (Figure S2A), the 61-kDa precursor was initially expressed at 4 h and continued until 36 h; however, the stable mature 51-kDa form first appeared at 12 h. To our surprise, the intermediate 57-kDa form was minimally expressed for a limited time (Figure S2A). The expression level of the 51-kDa protein was proportionate to that of the 61-kDa form, suggesting that the continuous presence of the precursor is necessary. Given the limited level of the 57-kDa intermediate form, it is likely that SCC is rapidly processed to the 51-kDa protein (Figure S2A) possibly because the 57-kDa intermediate is in an energetically unfavorable conformation. We quantitatively analyzed the expression level of SCC in three different states with

time (Figure 1K); the disappearance of the 61-kDa form after 36 h indicated its complete transit to the matrix. These results suggest the direct transport of the 61-kDa precursor to the 57-kDa intermediate, which is rapidly processed to a 51-kDa protein. The intermediate step is short lived and might be the regulatory step for mitochondrial processing.

SCC is highly expressed in adrenals and gonads. We studied the differences in the folding in all three states (precursor to intermediate to mature state) by density gradient separation of digitonin-lysed mitochondria from mouse testes and visualization by staining with SCC antibody. As shown in Figure S2B, the 61-kDa form was distributed in fractions 4–11, whereas the 57-kDa SCC was distributed from fractions 5–9. The narrower distribution and reduced intensity of the 57-kDa protein is suggestive of its rapid processing. Indeed, the 51-kDa form was first detected in fraction 6 (Figure S2C, red arrow). Distribution analysis showed that the 61-kDa protein was distributed for a longer time with a peak intensity at fraction 10. The 57-kDa protein form was observed from fraction 5, confirming a short delay in processing and the possible presence of an energetically unfavorable state (Figure 1L). Finally, the 51-kDa SCC form was observed from fraction 6, reaching maximum intensity at fraction 9 (Figure 1L). Staining the same fractions with an antibody specific for OMM-associated VDAC2 showed its expression reaching maximum intensity at fractions 6–10 (Figures S2C and 1M), confirming an accuracy of density preparation. These data suggest that the expression of the intermediate 57-kDa protein is limited and formation of the 51-kDa form is slower than that of the 57-kDa form.

Transient Stable Conformation at the Matrix

Because the intermediate 57-kDa form is a short-lived protein, we hypothesized that it was not completely folded and thus needed to be processed to the next stable folding state. We next evaluated ^{35}S-labeled SCC mitochondrial membrane integration using limited proteolysis, as the mitochondrial membrane transiently protects proteins from proteolysis but unimported or partially imported protein will be rapidly proteolyzed. Following import, mitochondria were incubated with proteinase K (PK), where the 51-kDa protein was insensitive to protease as compared with 57-kDa SCC, suggesting that it has a more open folding as compared with 51-kDa SCC (Figure 2A). As expected, 51-kDa SCC was partially proteolyzed in the presence of Triton X-100 owing to the increased access of PK with Triton micelles into the inner mitochondrial compartment, suggesting that this form was protected by mitochondria (Bose et al., 2019).

To understand the degree of membrane association by the 57- and 51-kDa proteins, we next identified the surface-exposed regions of SCC by proteolysis with trypsin, which cleaves after lysine and arginine residues under mildly alkaline conditions (pH $\geq$ 7.0). Proteins that are membrane integrated but loosely folded will be proteolyzed faster as compared with those tightly bound. As shown in Figure 2B, ^{35}S-SCC was synthesized and imported into isolated mitochondria from MA-10 cells followed by incubating with increasing concentrations of trypsin. The imported 57-kDa SCC was completely proteolyzed with 10 U of trypsin. The 61- and 51-kDa bands were resistant to proteolysis with up to 50 U of trypsin. Although the 61-kDa form was completely proteolyzed with 100 U of trypsin (Figure 2B), the 51-kDa SCC was resistant, indicating that mitochondrial integration shielded the 51-kDa protein, which may be tightly integrated into the membrane. Quantitative analysis of the mitochondrial processing efficiency (Figure 2C) suggests that rapid proteolysis of the 57-kDa protein may be due to a more open conformation or a partially unfolded state (Bose et al., 1999; Privalov, 1996). Thus, there is a difference in the folding between the 57- and 51-kDa SCC, with the 57-kDa protein folding as energetically unfavorable.

Folding Inside the Mitochondria Is Crucial

Mitochondrial import through the narrow protein import channel at the OMM requires at least partial unfolding at the cytoplasm either prior to import or during import (Neupert and Herrmann, 2007). We hypothesized that unfolded protein incubation with mitochondria may reach the final state faster during its import, as no additional time is necessary to unfold. However, if inner mitochondrial folding machinery is required then SCC may not reach the final step resulting in inactive protein. To examine this, we first unfolded SCC by incubating with urea prior to import into freshly isolated mitochondria from MA-10 cells. Addition of urea to SCC prior to import had no effect on import into mitochondria, as the intensity of the 57-kDa SCC band was unchanged (Figure 2D). However, the 51-kDa form of SCC was absent, suggesting that the first step processing from 61- to 57-kDa SCC is independent of protein folding, unlike the second step.

We next examined the mechanism required for activation from 57- to 51-kDa SCC using various metabolic inhibitors. Oligomycin (OLIGO) inhibits the H^+-translocating ATP, valinomycin (VAL) collapses the

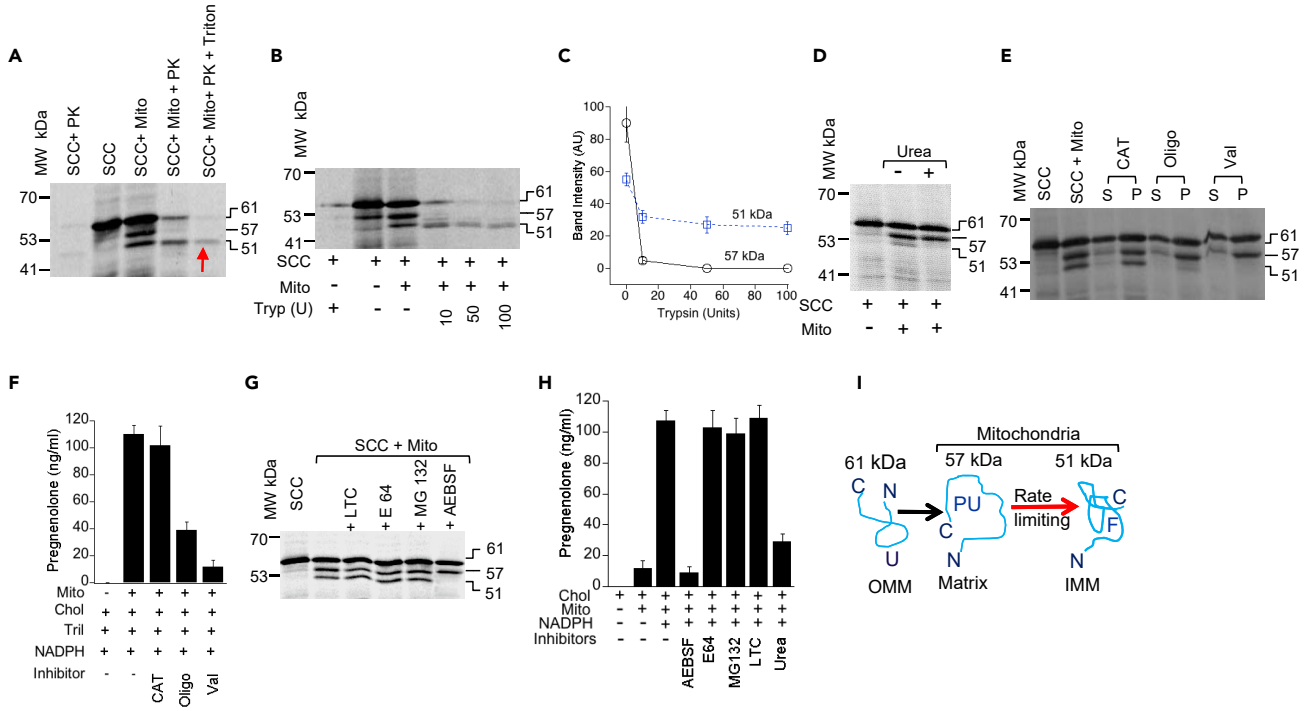

Figure 2. Intermediate Matrix Resident SCC Is the Active Regulatory Step

(A) Analysis of the mitochondrial import of ^{35}S-SCC in the presence and absence of proteinase K (PK) and Triton X-100 together and independently.

(B) ^{35}S-SCC import analysis following incubation with the indicated concentrations of trypsin.

(C) Quantitative analysis of ^{35}S-SCC, showing the imported 57- and 51-kDa fractions from (B).

(D) Import of ^{35}S-SCC protein into the isolated mitochondria from MA-10 cells in the presence and absence of urea.

(E) Import of ^{35}S-SCC in the presence of different uncouplers followed by separation of the membrane integrated fraction from the unimported fraction by extraction with sodium carbonate. The unimported and imported membrane integrated fractions are designated as S (supernatant or unimported) and P (pellet or imported).

(F) Determination of activity by measurement of ^{14}C-Cholesterol to pregnenolone conversion from the testicular mitochondria incubated with the indicated uncouplers: carboxyatractyloside (CAT), Oligomycin (Oligo), and Valinomycin (Val).

(G) Import analysis of ^{35}S-SCC protein into mitochondria that was preincubated with the indicated inhibitors.

(H) Determination of activity by measurement of ^{14}C-Cholesterol to pregnenolone conversion from mice testicular mitochondria incubated with AEBSF, E64, MG132, LTC, and Urea.

(I) Cartoon describing that unfolded 61-kDa SCC (U) was loaded at the OMM for import. Following import at the matrix, SCC domains remained partially unfolded (PU) and thus susceptible to faster proteolysis. In the next step, SCC is folded (F) and integrated at the IMM. The red arrow indicates that the rate limiting step of SCC is the transport of unfolded SCC from the matrix to IMM in folded form. (C), (F), and (H) are means ± SEM from three independent experiments performed three times.

electrochemical potential across the inner membrane, and carboxyatractyloside (CAT) inhibits access of ATP to the matrix. OLIGO and VAL, but not CAT, inhibited processing of 57-kDa SCC to 51-kDa SCC (Figure 2E). To further confirm that the processed 57-kDa protein remained membrane associated, we separated the imported from the unimported, following carbonate extraction, which shows that the imported 57-kDa protein remained in the pellet and was not free in solution (Figure 2E) because Na_2CO_3 at higher pH (pH ≤ 11.0) breaks protein-protein interaction but not the lipid-protein interaction (Li and Shore, 1992). In summary, 57- and 51-kDa forms are both membrane integrated.

When we next determined metabolic activity following incubation of carboxyatractyloside (102.3 ± 12.34 ng/mL and oligomycin 39.01 ± 5.4 ng/mL ($p = 0.087$), only oligomycin reduced activity more than 50% (Figure 2F). Quantitative analysis of the metabolic activity showed that it was reduced to 33–37 ng/mL with oligomycin as compared with 110 ± 7.2 ng/mL ($p = 0.044$) in the absence of any inhibitor (Figure 2F); it was further reduced with valinomycin to 11.5 ± 0.5 ng/mL ($p = 0.006$). As the inhibitors suppressed H+ circulation from the matrix to IMS, the processing of 57-kDa SCC to 51-kDa SCC requires an active force generated by the $\Delta\psi$, suggesting that 57-kDa protein cleavage requires an active membrane potential. Furthermore, the synthesis of a minimum amount of steroid in the presence of oligomycin was

confirmed due to the minimal synthesis of the 51-kDa band, which may have been generated owing to the leakage of protons across the chemical gradient.

Mass spectrometric analysis of the 400-kDa complex shows the presence of PIM1 protease (GeneBank: GI |256071912), a matrix resident protein. We also observed that the first step of import is independent of folding at the mitochondria (Figure 2D). This suggests that, after 57-kDa SCC is imported at the mitochondrial matrix following first step processing, it cannot interact appropriately with PIM1 protease (Savel'ev et al., 1998). During mitochondrial import of ^{35}S-SCC, we blocked PIM1 activity by preincubating mitochondria with the protease inhibitor (E64), proteosomal inhibitor (MG 132) and serine protease inhibitors, AEBSF (irreversible inhibitor), and leupeptin (LTC; reversible inhibitor). SCC processing from the 57- to 51-kDa form was not inhibited by E64, MG132, or LTC, but it was inhibited by AEBSF (Figure 2G). To understand further that the 51-kDa membrane-bound SCC is essential for activity, we have determined activity after incubating LTC, E64, MG132, and AEBSF with the isolated mitochondria from mouse testes. As expected, AEBSF resulted in no pregnenolone synthesis, suggesting that presequence cleavage is essential. Apart from the AEBSF treatment group in which 12 ng/mL pregnenolone was synthesized, all other protease inhibitor groups synthesized around 105 ng/mL pregnenolone; 23 ng/mL was synthesized in the presence of urea (Figure 2H). Thus, prior to localization at the OMM, the SCC precursor was unfolded (U) for passing through the import channel, although it was associated with the OMM. Without using the mitochondrial contact site and bypassing the IMS, SCC was integrated into the matrix with a partially open conformation (PU), which is then translocated at the IMM as a mature 51-kDa SCC (F) because the partially folded, membrane-integrated 57-kDa intermediate was proteolyzed rapidly in the presence of trypsin. So, the rate-limiting step for metabolic reaction initiation depends on the formation of 51-kDa SCC protein (Figure 2I).

The Intermediate State of Folding Is the Crucial Regulator

Although the acute regulation of steroid synthesis is rapid, it still requires minutes to cleave the side chain of cholesterol to form pregnenolone, which we consider an activation time of SCC necessary for catalysis. We hypothesize that SCC processing from the 57- to 51-kDa form is the rate-limiting step for the generation of active SCC. To test this hypothesis, we performed a mitochondrial import experiment with ^{35}S-SCC from 5 min to 2 h and found that the 57- to 51-kDa protein processing started immediately within 5 min and continued to 1 h (Figure 3A). Quantitative evaluation of the processing (Figure 3B) shows that the 57-kDa protein was 2.8 times more abundant than the 51-kDa SCC.

We next sought to determine the mechanism by which the equilibrium balance is maintained in the mitochondrial matrix in the presence and absence of energy requirements. We first incubated ^{35}S-SCC with isolated mitochondria from MA-10 cells or mouse testes in the absence of ATP and ADP. Only 57-kDa SCC but not the 51-kDa protein was present, suggesting that the first step of SCC can be imported in the absence of ATP. Because the processing of 57-kDa SCC increased with time, although the 51-kDa protein was absent completely, first step processing does not require energy from ATP (Figure 3C). The import efficiency remained unchanged at 26°C and 37°C (Figure 3D) as well as in the presence of a 40-fold difference in ATP concentration (Figures 3E and 3F). These data contrast with the ATP requirements for SCC mitochondrial processing (Boopathi et al., 2008; Chen and Douglas, 1987; Ondrovicova et al., 2005; Schleyer and Neupert, 1985; Suzuki et al., 1997) and also suggests that an activation mechanism of the 57-kDa is necessary to be processed to the next step in addition to $\Delta\Psi$ from the matrix to the IMS.

Succinate Activates Intermediate State Folding

Anionic succinic acid acts as a metabolic intermediate; it is converted into fumarate by succinate dehydrogenase in complex II of the ETC in ATP generation. Succinate anion is also responsible for respiration and mitochondrial membrane potential (Gullans et al., 1988); thus, it might be responsible for the circulation of energy across the IMS. We performed a kinetic study of SCC processing with varying concentrations of succinate added to the mitochondrial import reaction, which was preincubated with ATP for 30 min before the addition of succinate. We have observed the 51-kDa protein appeared after addition of 0.2mM succinate; however, further increases in succinate concentration did not increase 57- to 51-kDa SCC processing, suggesting that there is a limited availability of 57-kDa SCC to be processed to the mature form (Figure 3G). Quantitative analysis shows that the intensity of the 51-kDa band was 3.4-fold lower as compared with the 57-kDa protein (Figure 3H). However, when succinate was added at the start of the import reaction, the intensity of distribution between the 57- and 51-kDa bands was significantly lower (Figure 3I) as compared

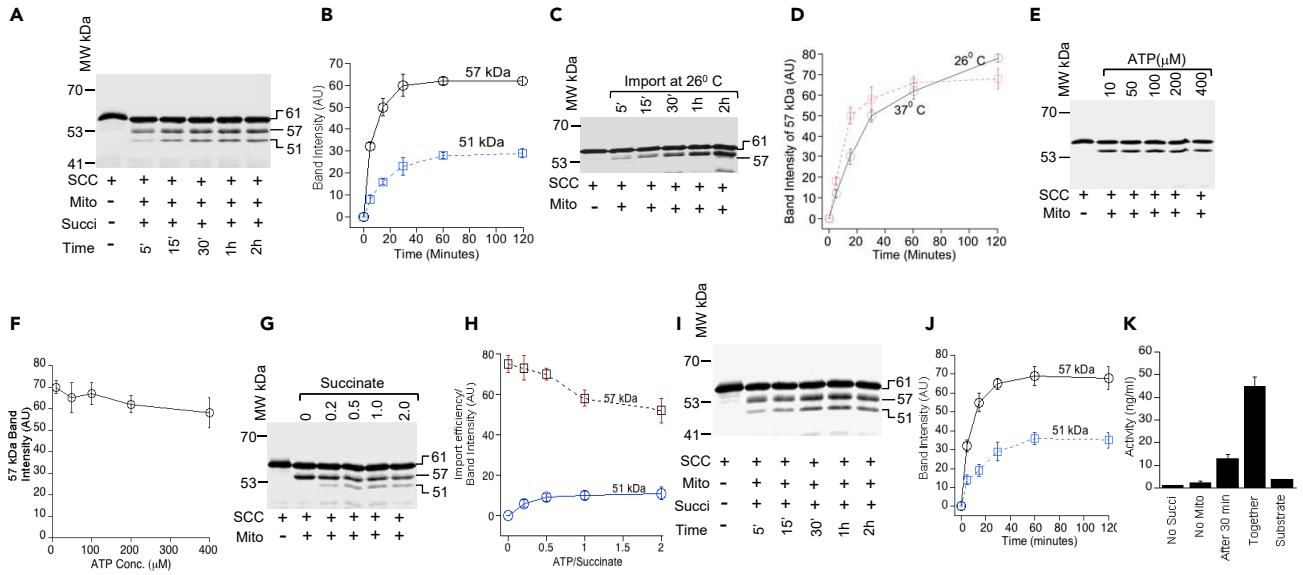

Figure 3. Succinate and ATP Combination Is Essential for SCC Processing and Activity

(A) Analysis of mitochondrial import kinetics of ^{35}S-SCC following incubation at 26°C for the indicated time.

(B) Measurement of the intensity of 57-kDa (solid black line with open round circle) and 51-kDa (dotted blue line with open squares) import from (A).

(C) Analysis of ^{35}S-SCC import into isolated mitochondria at the indicated time in the absence of ATP and succinate.

(D) Quantitative measurement of the formation of 57-kDa SCC after import at 26°C and 37°C.

€ Analysis of ^{35}S-SCC import into isolated mitochondria with a 40-fold difference in ATP concentration.

(F) Quantitative measurement of the formation of 57-kDa SCC from (E).

(G) Analysis of ^{35}S-SCC import into isolated mitochondria at the indicated time in the presence of ATP and succinate.

(H) Quantitative analysis of the intensity of 57- and 51-kDa SCC from (G).

(I) Analysis of ^{35}S-SCC import into isolated mitochondria at the indicated time, where after 1 h of import (time 0 min) succinate was added with increasing concentration and then imported for an additional 1 h.

(J) Quantitative measurement of ^{35}S-SCC import from (I), where the 57-kDa (black solid line with circle) and 51-kDa (blue broken line with square) SCC are shown.

(K) Measurement of activity (progesterone) when succinate was added together with ATP or after 0.5 h. Data in (B), (D), (F), (H), (J), and (K) are means ± SEM from three independent experiments, each performed in triplicate.

See also Figure S3.

with later addition of succinate (Figure 3G), suggesting that the presence of succinate is essential for SCC cleavage. Comparing the difference in cleavage between the immediate addition of succinate and delayed addition after starting the mitochondrial import reaction revealed that the 51-kDa form was 4-fold higher at 30 min (Figure 3J). Thus, succinate may facilitate an active conformation in the presence of ATP, which is dependent on H^+ availability to generate the active state of folding for 57-kDa SCC. In addition, SCC activity was ~3.3-fold lower following addition of succinate after 30 min (Figure 3K). Quantitative analysis of the amount of progesterone synthesized shows that 12.4 ± 2 ng/mL of progesterone was produced as compared with 43 ± 3.8 ng/mL ($p = 0.065$) of progesterone when succinate was added at the beginning of the reaction (Figure 3K). Hence, 51-kDa SCC is dependent on the availability of active 57-kDa SCC, which is generated in the presence of succinate anion, suggesting that succinate anion provides a translocation potential from the matrix.

Succinate Drives the Mitochondrial Complex Stabilization

Succinate is a product of substrate-level phosphorylation in the citric acid cycle by donating a pair of electrons. We hypothesize that succinate may facilitate SCC activity through stabilization of the mitochondrial complex. We next examined the different stable states of mitochondrial metabolic activity as measured by the total enthalpy (ΔH) using titration calorimetry with increasing concentrations of succinate to mitochondria isolated from the MA-10 cells or testicular tissues. The negative (ΔH) indicates stabilization, whereas a positive (ΔH) is an unstable or a less stable state. We observed that ΔH continuously decreased with increasing succinate concentration up to 25mM (−5.6 ± 1.4) where it is saturated, suggesting that all the available substrates from mitochondria are consumed (Figure 4A).

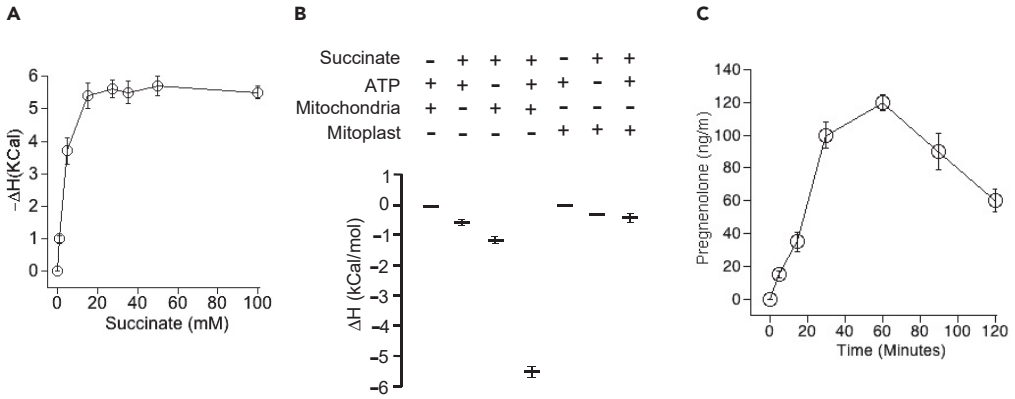

Figure 4. Stabilization of SCC-Associated Mitochondrial Complex

(A) Measurement of ΔH by isothermal titration calorimetry with indicated concentrations of succinic acid to the fixed 20 μg of testicular mitochondria containing external addition of 10 mM ATP.

(B) Measurement of ΔH by isothermal titration calorimetry. ΔH was measured with 20 μg of mitochondrial protein or from 20 μg of mitoplast protein and in the presence of 10 mM ATP and 50 mM succinate at 37°C for 1 h.

(C) Quantitative measurement of activity (^{14}C-cholesterol to pregnenolone conversion) with mitochondria isolated from MA-10 cells over different period of time.

See also Figure S4.

To examine if succinate anions stabilize complex II, we determined the change in heat content following addition of succinate and/or ATP to mitochondria or mitoplasts. Titration calorimetry showed that the enthalpy decreased in the presence of both ATP and succinate to –ΔH 5.82 kCal/mol in 1 h. However, in any other combination, the enthalpy (ΔH) was 0.32 to – 1.2 kCal/mol (Figure 4B) at the same time. As the absence of succinate inhibited the circulation of H^+ from the matrix to IMS, the processing of 57-kDa to 51-kDa SCC requires an active force generated by the Δψ. Thus, 57-kDa SCC cleavage requires an active membrane potential. The presence of succinate ions remained unchanged in mitochondria and mitoplasts; however, the enthalpy was reduced (stabilized) in the presence of mitochondria, suggesting that the generation of a mitochondrial proton pump is dependent on the presence of ATP and succinate together from the matrix to the IMS.

To confirm that indeed a new pool of active 51-kDa SCC is necessary for maximum activity, we determined pregnenolone synthesis over time using ^{14}C-cholesterol and MA-10 mitochondrial lysates. As shown in Figure 4C (Figure S3A), activity is detected within 15 min, reaching maximal activity within 1 h followed by decreased activity possibly due to a lack of active 51-kDa SCC. Quantitative analysis of pregnenolone synthesis showed 37, 100, and 126 ng/mL pregnenolone at 5, 15, and 30 min, respectively (Figure 4C). Pregnenolone levels decreased to 36 ng/mL after 2 h, suggesting that all the substrate was used and that no more active 51-kDa SCC was available despite the presence of succinate and ATP (Figure 4C).

The succinate anion participates in complex II, suggesting that the availability of the active complex became saturated at 1 h possibly due to limited stability. To confirm this hypothesis, we performed an import experiment using ^{35}S- wild-type and mutant A359V SCC into freshly isolated mitochondria in the presence and absence of ATP and/or succinate. Purification of the imported reactions followed by solubilization with digitonin and analysis through a native gradient PAGE showed both the wild-type and mutant formed similar-sized complexes (Figure 5A), because the wild-type and mutant SCC proteins are processed into the mitochondria in an identical fashion (Bose et al., 2019). However, in the absence of succinate, the complex size was reduced significantly (Figure 5B) along with the reduced activity of the complex (Figures 5C and S4). Quantitative analysis showed that 14 ± 1.3 ng/mL of progesterone was synthesized in the absence of succinate as compared with 64 ± 5.8 ng/mL ($p = 0.079$) in the presence of succinate (Figure 5C), suggesting that succinate is essential to generate the SCC network of interaction. The limited activity in the absence of succinate may be due to leakage of protons or crude complex isolation. In summary, succinate stabilized the mitochondrial complex, resulting in increased activity.

To further confirm that succinate alone plays the central role in regulating the SCC complex, we permanently knocked down malate dehydrogenase (MDH2) in MA-10 cells with the silencing vector, which

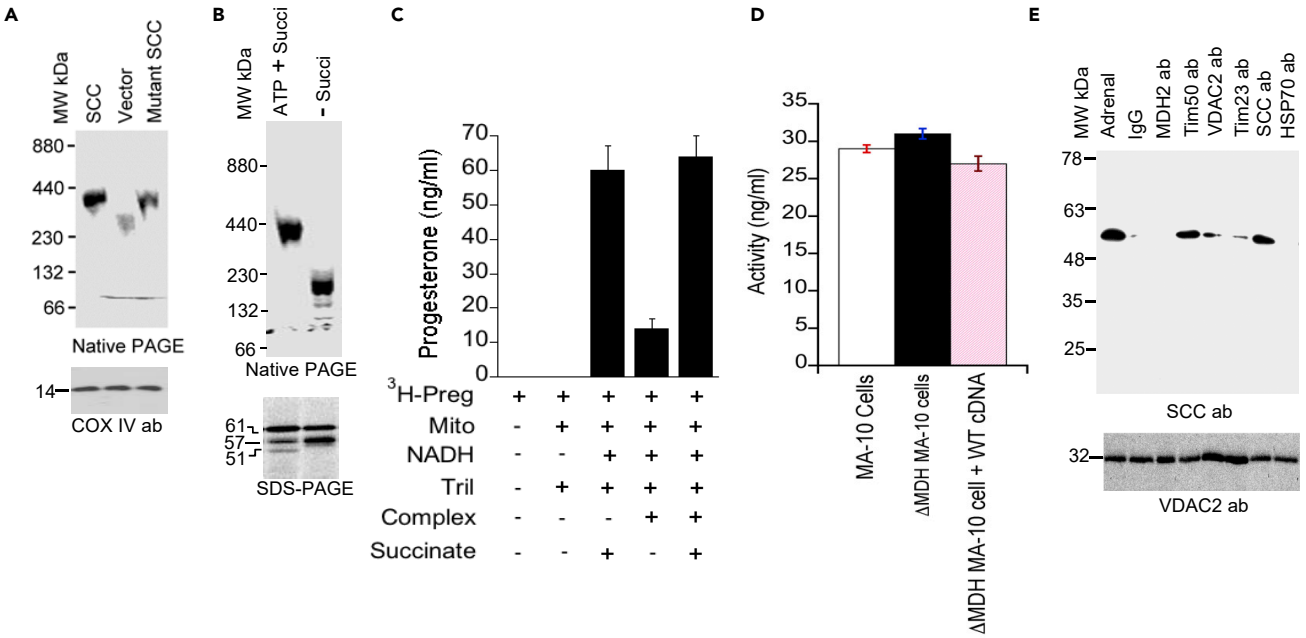

Figure 5. SCC-Associated Mitochondrial Protein Network in Steroid Metabolism

(A) Native gradient PAGE analysis of the digitonin-solubilized mitochondrial import complex of the wild-type ^{35}S-SCC and mutant ^{35}S-A359V SCC in MA-10 cells.

(B) Native gradient PAGE analysis of the digitonin-solubilized mitochondrial import complex following ^{35}S-SCC import into mitochondria at the indicated composition of ATP and succinate, together or independently.

(C) Activity of the digitonin-solubilized complex.

(D) Activity of the malate dehydrogenase knockdown MA-10 cells and its comparison following co-transfection of wild-type cDNA of the knockdown cells. Trilostane (Tril) was added to inhibit 3βHSD2 activity to stop conversion after pregnenolone.

(E) Co-immunoprecipitation of lysate from MA-10 cells with the indicated antibodies followed by western blotting with SCC antibody. Bottom panel is the western blot of the lysates applied in each reaction. Data in (C) and (D) are means ± SEM from three independent experiments, each performed in triplicate. See also Figure S5.

does not affect expression of other mitochondrial proteins as seen by unchanged expression in PDC protein of pyruvate dehydrogenate complex (PDC-E2) (Figure S5). We next determined activity and interaction of MDH2 with SCC. Measurement of activity showed no difference in activity of the knockdown cells from mouse Leydig MA-10 cells or with the insertion of another copy of MDH2 cDNA into the knockdown cells (Figure 5D). Next, to examine malate dehydrogenase interaction with SCC in the native state within cells, we performed co-immunoprecipitation experiments with digitonin-solubilized native complexes isolated from the mitochondria of MA-10 cells. Mitochondrial translocase Tim50 interacts strongly with SCC (Bose et al., 2019) and also showed minimal interaction with inner mitochondrial translocase Tim23 and outer mitochondrial resident VDAC2 (Figure 5E). However, we find no interaction with malate dehydrogenase suggesting that SCC is not close to malate dehydrogenase. Tim50 regions at the IMM interact with SCC possibly because of a reversible change in conformation required between SCC and other mitochondrial translocases (Bose et al., 2019) but not the malate dehydrogenase. The staining of lysate with VDAC2 antibody independently confirmed the presence of an equivalent amount of lysate in each reaction (Figure 5E, bottom). Hence, malate dehydrogenase has no direct role in the complex II associated with SCC.

DISCUSSION

The liver is the principal organ involved in *de novo* synthesis of cholesterol from acetyl-CoA, although most cell types, including adrenal cortex and testicular steroidogenic cells, can synthesize cholesterol (Miller and Bose, 2011). Glycolysis produces ATP required for synthesis of cytosolic acetyl-CoA. The different genes involved in glycolysis, the TCA cycle, oxidative phosphorylation, and steroidogenesis are also activated at the same time (Inoue et al., 2016). As steroidogenic cells do not store steroids, to synthesize large amounts of steroid on demand, they must rapidly synthesize steroids by coordinating multiple routes that supply the materials for immediate synthesis.

Steroid synthesis is initiated by cholesterol side-chain cleavage by SCC inside the mitochondria. In adrenal and gonadal mitochondria, mature and active 51-kDa SCC integrates with the IMM, interacting with the coactivators, ferredoxin and ferredoxin reductase, to carry out the metabolic reaction. Ferredoxin reductase is a soluble protein highly expressed in steroidogenic tissues and is associated with the IMM (Hanukoglu, 1992; Lambeth et al., 1979). The crystal structure of both ferredoxin and ferredoxin reductase shows a charge segregation rendering cleft where one side is positively charged and the other side is negatively charged (Ziegler et al., 1999). Thus, the binding affinity between ferredoxin and ferredoxin reductase could arise from a long-range interaction in the SCC-specific complex (Brandt and Vickery, 1993). As a result, the interaction with complex II may result in the folded state of the 51-kDa protein.

Complex formation requires the appropriately folded 51-kDa protein not an intermediate state pseudostable 57-kDa protein. Blocking the formation of 51-kDa SCC by AEBSF or valinomycin completely ablated activity. In the absence of succinate or mitochondria with urea, no activity was observed. In the absence of succinate, the complex did not contain the IMM-integrated protein, Tim23, suggesting that 51-kDa SCC folding is required to form a network with the TIM23 complex (Bose et al., 2019). Any disturbance in the thermodynamic equilibration disrupts the complex, ablating the ETC electron transport system activity.

Complex I electron transport is critical for premature electron transport and steroidogenesis initiation because SCC activity was inhibited in the presence of the complex I inhibitor, rotenone (Bose et al., 2008). In complex II, additional electrons are delivered into the quinone pool, originating from succinate, and proceed through four different subunit complex reactions. Succinate is generated from the succinyl-CoA in the TCA cycle via succinyl-CoA ligase. We found that the 57-kDa SCC intermediate state requires activation by succinate anions in the presence of ATP (Figure 4A), suggesting that circulating phosphate maintains the intermediate state active. This is possible if the 57-kDa intermediate remains in a conformation to accept circulating phosphates from ATP. Thus, the intermediate may be in a partially open conformation as compared with the finally folded conformation, 51-kDa SCC. In the absence of succinate anion, 57-kDa intermediate SCC is not activated despite the presence of ATP and coactivators in the matrix. Thus, succinate activated complex II to participate with complex III in the electron transport cycle to maintain the steroid metabolic process for survival.

In conclusion, we show here that SCC is directly loaded onto the OMM, (1) transferred to the matrix, (2) processed to an intermediate state independent of ATP that was partially open, which (3) was finally integrated with the IMM as an active protein. (4) Formation of the active SCC (51-kDa) form is dependent on the availability of the active intermediate state. (5) Inhibition of the protease activity or change of intermediate state of folding ablates activity. (6) Holding at the intermediate state suggests that the active 51-kDa SCC depends on the intermediate state, and, thus, it is the rate-limiting step. (7) The proton pump circulates energy from the matrix to the IMS and dissipates it in the absence of the OMM. (8) The 51-kDa conformation is an energetically stable state to initiate the metabolic reaction in the presence of succinate and ATP; inhibition of succinate reduces phosphate circulation, complex formation, and activity. Succinate is responsible to move the ETC complex II (Figure 6); thus, SCC is activated from complex II to participate with complexes III and IV to induce metabolic reactions.

Limitations of the Study

We showed direct measurement of complex stability through calorimetry and biochemical experiments. The stability of the complex depends on its preparation and measurement of activity, and mostly noise level around the calorimeter. The activity measurement is more reproducible with the mitochondrial complex isolated from adrenals and testes, as compared with ovaries. The mitochondrial complex conducted with electrophysiology would be supportive, but this is beyond the scope of our resources.

Resources Availability

Lead Contact

Further information and requests for resources and reagents should be directed to and will be fulfilled by the Lead Contact, Himangshu S. Bose (Bose_hs@mercer.edu).

Materials Availability

This study did not generate new unique reagents. Reagent request will be readily fulfilled following the materials transfer policies of Mercer University School of Medicine.

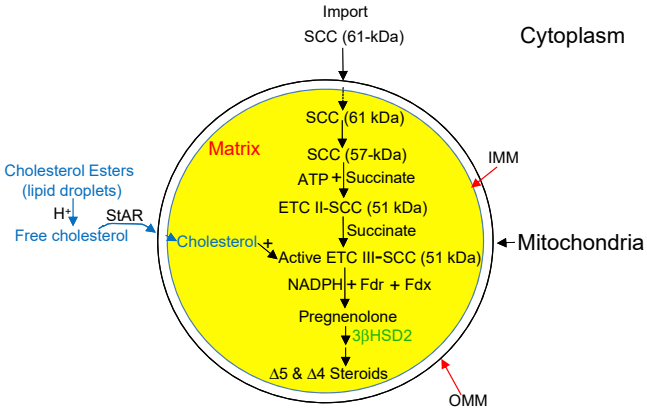

Figure 6. Schematic Presentation of ETC Complex III Activation

SCC is synthesized as a 61-kDa protein in the cytoplasm (ER free ribosomes) and directly transported to the mitochondria, where it is processed to a 57-kDa intermediate protein. In the next step, this 57-kDa SCC with succinate anion and ATP is processed to an active 51-kDa protein, generating complex II. In the next step, this active SCC in complex II is processed to generate active complex III, where SCC cleaves the already imported side chain of cholesterol with the help of electron-donating partners NADPH, Ferredoxin (Fdr), and Ferredoxin reductase (Fdx) generating pregnenolone. Pregnenolone is then catalyzed by 3βHSD2 in the next family of steroid synthesis (Δ5 and Δ4 steroid).

Data and Code Availability

This study did not generate any new computational program or structure or sequencing data.

METHODS

All methods can be found in the accompanying Transparent Methods supplemental file.

SUPPLEMENTAL INFORMATION

Supplemental Information can be found online at https://doi.org/10.1016/j.isci.2020.101295.

ACKNOWLEDGMENTS

H.S.B. was supported by grants from American Heart Association (09GRNT2190059), National Institutes of Health (HD057876), Navicent Foundation (570257), and a seed grant from Mercer University. H.S.B. is thankful to Drs. Mahuya Bose and Wei-Hsiung Yang for critically reading the manuscript.

AUTHOR CONTRIBUTIONS

H.S.B. conceptualized and designed the research. H.S.B., R.M.W., D.K.D., B.M., and E.W.P. performed research. B.M. analyzed electron microscopy, and R.M.W. performed mass spectrometry experiments and analyzed results. H.S.B. analyzed the data and wrote the paper. HSB and DKD performed part of the experiment at the U of Florida, Gainesville, FL. The complete manuscript was available to all the authors prior to submission and they agreed with the final version of the manuscript.

DECLARATION OF INTERESTS

The authors declare that they do not have any conflicts of interest. They also declare that they do not have any financial interests.

Received: January 7, 2020
Revised: April 23, 2020
Accepted: June 15, 2020
Published: July 24, 2020

REFERENCES

Boopathi, E., Srinivasan, S., Fang, J.K., and Avadhani, N.G. (2008). Bimodal protein targeting through activation of cryptic mitochondrial targeting signals by an inducible cytosolic endoprotease. Mol. Cell *32*, 32–42.

Bose, H.S., Gebrail, F., Marshall, B., Perry, E.W., and Whittal, R.W. (2019). Inner mitochondrial translocase Tim 50 is central in adrenal and testicular steroid synthesis. Mol. Cell. Biol. *39*, https://doi.org/10.1128/MCB.00484-00418.

Bose, H.S., Sugawara, T., Strauss, J.F., III, and Miller, W.L. (1996). The pathophysiology and genetics of congenital lipoid adrenal hyperplasia. N. Engl. J. Med. *335*, 1870–1878.

Bose, H.S., Whittal, R.M., Baldwin, M.A., and Miller, W.L. (1999). The active form of the steroidogenic acute regulatory protein, StAR, appears to be a molten globule. Proc. Natl. Acad. Sci. U S A *96*, 7250–7255.

Bose, M., Whittal, R.M., Miller, W.L., and Bose, H.S. (2008). Steroidogenic activity of StAR requires contact with mitochondrial VDAC1 and phosphate carrier protein. J. Biol. Chem. *283*, 8837–8845.

Brandt, M.E., and Vickery, L.E. (1993). Charge pair interactions stabilizing ferrodoxin-ferrodoxin reductase complexes. J. Biol. Chem. *268*, 17126–17130.

Chen, W.J., and Douglas, M.G. (1987). Phosphodiester bond cleavage outside mitochondria is required for the completion of protein import into the mitochondrial matrix. Cell *49*, 651–698.

Chung, B., Matteson, K.J., Voutilainen, R., Mohandas, T.K., and Miller, W.L. (1986). Human cholesterol side-chain cleavage enzyme, P450scc: cDNA cloning, assignment of the gene to chromosome 15, and expression in the placenta. Proc. Natl. Acad. Sci. U S A *83*, 8962–8966.

Ding, T., Hardiman, P.J., Petersen, I., Wang, F.-F., Qu, F., and Baio, G. (2017). The prevalence of polycystic ovary syndrome in reproductive-aged women of different ethnicity: a systematic review and meta-analysis. Oncotarget *8*, 96351–96358.

Gullans, S.R., Kone, B.C., Avison, M.J., and Giebisch, G. (1988). Succinate alters respiration, membrane potential, and intracellular K+ in proximal tubule. Am. J. Physiol. *255*, F1170–F1177.

Guo, Y., Xie, C., Li, X., Yang, J., Yu, T., Zhang, R., Zhang, T., Saxena, D., Snyder, M., Wu, Y., et al. (2017). Succinate and its G-protein-coupled receptor stimulates osteoclastogenesis. Nat. Commun. https://doi.org/10.1038/ncomms15621.

Hanukoglu, I. (1992). Steroidogenic enzymes: structure, function, and role in regulation of steroid hormone biosynthesis. J. Steroid Biochem. Mol. Biol. *43*, 779–804.

Hayaski, T., Rizzuto, R., Hajnoczky, G., and Su, T.P. (2009). MAM: more than just a housekeeper. Trends Cell Biol. *19*, 81–88.

He, W., Miao, F.J., Lin, D.C., Schwandner, R.T., Wang, Z., Gao, J., Chen, J.L., Tian, H., and Ling, L. (2004). Citric acid cycle intermediates as ligands for orphan G-protein-coupled receptors. Nature *429*, 188–193.

Inoue, M., Shima, Y., Miyabayashi, K., Tokunaga, K., Sato, T., Baba, T., Ohkawa, Y., Akiyama, H., Suyama, M., and Morohashi, K. (2016). Isolation and characterization of fetal Leydig progenitor cells of male mice. Endocrinology *157*, 1222–1233.

Itakura, E., Zavodszky, E., Shao, S., Wohlever, M.L., Keenan, R.J., and Hegde, R.S. (2016). Ubiquilins chaperone and triage mitochondrial membrane proteins for degradation. Mol. Cell *63*, 21–33.

Kaur, J., Rice, A.M., O'Conner, E., Piya, A., Buckler, B., and Bose, H.S. (2016). Novel SCC mutation in a patient of Mexican descent with sex reversal, salt-losing crisis and adrenal failure. Endocrinol. Diabetes Metab. https://doi.org/10.1530/EDM-16-0059.

Lambeth, J.D., Seybert, D.W., and Kamin, H. (1979). Ionic effects on adrenal steroidogenic electron system. J. Biol. Chem. *254*, 7255–7264.

Li, J.M., and Shore, G.C. (1992). Reversal of the orientation of an integral protein of the mitochondrial outer membrane. Science *256*, 1815–1817.

Matsumoto, M., Suzuma, K., Maki, T., Kinoshita, H., Tsuiki, E., Fujikawa, A., and Kitaoka, T. (2012). Succinate increases in the vitreous fluid of patients with active proliferative diabetic retinopathy. Am. J. Ophthalmol. *153*, 896–902.

Miller, W.L. (2017a). Disorders in the initial steps in adrenal steroidogenesis. J. Steroid Biochem. Mol. Biol. *165*, 18–37.

Miller, W.L. (2017b). Steroidogenesis: unanswered questions. Trends Endocrinol. Metab. *28*, 771–793.

Miller, W.L., and Auchus, R.J. (2011). The molecular biology, biochemistry, and physiology of human steroidogenesis and its disorders. Endocr. Rev. *32*, 81–151.

Miller, W.L., and Bose, H.S. (2011). Early steps in steroidogenesis: intracellular cholesterol trafficking. J. Lipid Res. *52*, 2111–2135.

Neupert, W., and Herrmann, J.M. (2007). Translocation of proteins into mitochondria. Annu. Rev. Biochem. *76*, 723–729.

Ondrovicova, G., Liu, T., Singh, K., Tian, B., Li, H., Gakh, O., Perecko, D., Janata, J., Granot, Z., Orly, J., et al. (2005). Cleavage site selection within a folded substrate by the ATP-dependent Lon protease. J. Biol. Chem. *280*, 25103–25110.

Prasad, M., Pawlak, K.J., Burak, W.E., Perry, E.E., Marshall, B., Whittal, R.M., and Bose, H.S. (2017). Mitochondrial metabolic regulation by GRP78. Sci. Adv. *3*, e1602038.

Privalov, P.L. (1996). Intermediate states in protein folding. J. Mol. Biol. *258*, 707–725.

Savel'ev, A.S., Novikova, L.A., Kovaleva, I.E., Luzikov, V.N., Neupert, W., and Langer, T. (1998). ATP-dependent proteolysis in mitochondria. m-AAA protease and P1M1 protease exert overlapping substrate specifies and coperate with the mtHsp70 system. J. Biol. Chem. *273*, 20596–20602.

Schleyer, M., and Neupert, W. (1985). Transport of proteins into mitochondria: translocation intermediates spanning contact sites between outer and inner membranes. Cell *43*, 339–350.

Shan, B., Long Zhou, L., Yang, S., Yan, M., Wang, Z., Ouyang, Y., Yao, S., Jin, T., and Li, Z. (2016). Association between polycystic ovary syndrome (PCOS) and CYP11A1 polymorphism in Hainan, China: a case-control study. Int. J. Clin. Exp. Pathol. *9*, 230–236.

Suomalainen, A., and Battersby, B.J. (2017). Mitochondrial diseases: the contribution of organelle stress responses to pathology. Nat. Rev. Mol. Cell Biol. *19*, 77–92.

Suzuki, C.K., Rep, M., van Diji, J.M., Suda, K., Grivell, L.A., and Schatz, G. (1997). ATP-dependent proteases that also chaperone protein biogenesis. Trends Biochem. Sci. *22*, 118–123.

Vafai, S.B., and Mootha, V.K. (2012). Mitochondrial disorders as windows into an ancient organelle. Nature *491*, 374–383.

Ziegler, G.A., Vonrheim, C., Hanukoglu, I., and Schulz, G.E. (1999). The structure of adrenodoxin reductase of mitochondrial P450 systems: electron transfer for steroid biosynthesis. J. Mol. Biol. *289*, 981–990.

iScience, Volume *23*

Supplemental Information

Electron Transport Chain Complex II Regulates Steroid Metabolism

Himangshu S. Bose, Brendan Marshall, Dilip K. Debnath, Elizabeth W. Perry, and Randy M. Whittal

1 **SUPPLEMENTAL INFORMATION**

Transparent Methods

Cell proliferation and isolation of mitochondria from tissues

MA-10 cells (Mouse Leydig) were cultured in Weymouth media (Sigma, St. Louis, MO) in the presence of 1X L-Glutamine, 10% horse serum and 5% FBS. Cells were kept at 37˚C in a humidified incubator with 5% CO_2 and mitochondria were isolated as described before (Bose et al., 2002). Sheep Adrenal glands, were obtained from the University of Florida, Gainesville, Animal Science Department, immediately after sacrifice. Tissues were diced in an ice-cold mitochondria isolation buffer containing 250mM sucrose (Bose et al., 2008), and mitochondria were isolated using a hand-held, all glass Dounce homogenizer following a previously described protocol (Bose et al., 2008). Most of the experiments were carried out with freshly isolated mitochondria from either cells or tissues. Malate dehydrogenase knockdown in MA-10 cells was performed with the silencing vector from Open Biosystem (Santa Cruz Biotechnology) and the knockdowns were selected with the antibiotic (50 μg/ml) hygomycin. Out of the five plasmids provided by the manufacturer only two plasmids were able to knockdown, as determined by western blotting with MDH2 antibody (Santa Cruz).

Isolation and fractionation of mitochondria

Mitochondria were isolated from mouse testis or sheep adrenals or cultured MA-10 cells by differential centrifugation as described previously (Bose et al., 2008). Mitochondrial pellets were resuspended in a 1:1 mix buffer and kept on ice. Mitoplasts were prepared by solubilizing the outer mitochondrial matrix (OMM) in 1.2 % (w/v) digitonin, a non-ionic detergent. Prior to digitonin treatment, mitochondria were incubated with 10mM HEPES (pH 7.4) for 5 min and centrifuged at 10,000 ×g for 20 min to separate the OMM from the inner mitochondrial matrix (IMM) and matrix (mitoplast). The OMM fraction was centrifuged at 130,000 ×g for 1 h to separate unimported SCC from the pellet membranes. IMM and matrix fractions were prepared by the treatment of mitoplasts with 0.16 mg of non-ionic lubrol (Ragan et al., 1986) per mg of mitochondria followed by ultracentrifugation at 130,000 ×g for 1 h. The soluble fraction was referred to as the matrix and insoluble part as the IMM, although it should be noted that this fraction also contains some intermembrane space (IMS) components. The matrix fraction

(supernatant) was removed, and the membrane pellet was resuspended in 1:1 mix buffer and kept on ice. The volume of the supernatant was measured, and the membrane pellet was resuspended in 1:1 mix buffer.

Western blot

For native Western staining, mitochondria were isolated from rat adrenal or testicular tissues or from the MA-10 cells following our previously described procedure (Pawlak et al., 2011a). The native complex was isolated by incubating mitochondria with buffer containing 1% digitonin, and samples were separated by electrophoresis through 4-16% native gradient gels. For denatured Western blotting, 12.5 mg of total or mitochondrial proteins were loaded per well. After the protein complexes from the native PAGE or SDS-PAGE were transferred to a polyvinylidine difluoride (PVDF) membrane, they were blocked with 3% nonfat dry milk for 45 min, probed overnight with the primary antibodies, and then incubated with peroxidase-conjugated goat anti-rabbit IgG or anti mouse IgG (Pierce, Rockford, IL). Signals were developed with a chemiluminescent reagent (Pierce). For direct visualization of the complexes, the gels were stained with Serva blue or Coomassie blue stain overnight at 4 °C. Unless otherwise indicated, antibodies to P450c11AS, VDAC2, and StAR were all purchased from Santa Cruz Biotechnology (Santa Cruz Biotech, Dallas, TX) or AbCam (Boston, MA). For antibody shift experiment, MA-10 cells were stimulated with cAMP for 18 h and then the mitochondria were isolated as described above. The mitochondrial pellet was solubilized with 1% digitonin, and then specific antibody was added at a previously determined dilution for 60 min. The antibody complex was isolated by centrifugation at 9000 rpm (Beckman Allegra 22XR, F630 rotor) for 45 min, resolved by 4 to 16% native gradient PAGE, transferred to a PVDF membrane, and western blotted with specific antibodies as described previously (Prasad et al., 2017).

***In vitro* synthesis and processing of the precursor protein with different mitochondrial fractions**

The full-length SCC cDNA was subcloned in SP6 vector and the protein was translated in a rabbit reticulocyte transcription translation system in the presence of ^{35}S-labeled methionine following manufacturer's instructions (Promega, Madison, WI). Freshly isolated mitochondria were incubated with a ^{35}S-labeled SCC or mutant SCC at 26˚ C for 1 h or as needed. The imported fractions were separated

from the unimported fraction by extraction with sodium carbonate as described previously (Bose et al., 2002). The membrane integrity was determined by proteolysis with proteinase K as described previously (Bose et al., 2019; Bose et al., 2002).

To confirm that the unimported form is not an aggregate, we performed ultracentrifugation of cell free transcription translation system (CFS) at 144,000 ×g before incubation with mitochondria. Partial proteolysis was performed with PK or trypsin independently with varying concentrations from 10 μg to 250 μg for PK and 1 to 100 Units of sequencing grade trypsin (Thermo Fisher). The import reactions were carried out at 26˚ C. In some experiments import reactions were carried out at different temperatures and also in presence of different inhibitors where Oligomycin 50 μg/mL, valinomycin 2.0 μg/mL and atractloside (CTL) 50 μg/mL were added just prior to start ^{35}S-SCC mitochondrial import. Similarly to study preunfolded ^{35}S-SCC was incubated with 1.0M urea in 10mM Tris buffer pH 7.4 and incubated with the freshly isolated mitochondria from MA-10 cells and import reactions were carried out at 26˚ C for 1 h and terminated by adding mCCCP.

For analysis of the assembled proteins in the complex, mitochondria from the transfected cells or testicular tissues were re-isolated and lysed in digitonin buffer (1% digitonin, 20mM Tris-HCl, pH 7.4, 0.1mM EDTA, 50mM NaCl, 10% glycerol, 1mM phenylmethylsulfonyl fluoride) for 15 min on ice. The digitonin lysate was combined with native-PAGE sample buffer (5% Coomassie Brilliant Blue G-250, 100mM BisTris, pH 7.0, 500mM 6-aminocaproic acid) and subjected to 4–16% or 6-13% gradient native-PAGE at 100 V overnight at 4° C. The native page was stained following electrophoresis to avoid any aberrant complex. Protein complexes were further fractionated by applying 100 μL of digitonin lysate to a 30-10% sucrose density step gradient, with a 200-μL 66% sucrose cushion at the bottom (final volume = 2.0 mL). Following centrifugation at 55,000 × *g* in a Beckman TLA55 rotor for 4 h, the sample was immediately equally aliquoted and loaded onto gradient, native-PAGE or SDS-PAGE gels. Radiolabeled proteins were detected by autoradiography or on a phosphorimager.

Expression kinetics of SCC in COS-1 cells

SCC cDNA was subscloned in the pCMV vector as described previously (Bose et al., 2019), and plasmid cDNA was purified through Qiagen Midi prep columns (Qiagen, Frederick, MD) following the manufacturer's procedure. Briefly, 1×10^6 COS-1 cells were cultured onto a six-well plate 14 h before the transfection, and 2 μg of cDNA was transfected in 3 wells using Lipofectamine (Thermo Fisher, Waltham, MA) as previously described (Bose et al., 2008). Following replacement of medium containing serum and antibiotics, cells were collected in every 4 h, and the SCC expression was determined by Western blotting with a SCC antibody (a kind gift from Dr. Bon-Chu Chung).

Mitochondrial viability analysis

We determined mitochondrial viability isolated from MA-10 cells or from rat testis following a recently developed procedure (Marriott et al., 2012; Prasad et al., 2016). In brief, mitochondrial membrane responsiveness was determined using an ATP Assay System Bioluminescence Detection Kit (ENLITEN, Promega) with a Veritas microplate luminometer (Turner Biosystems, Sunnyvale, CA) following the manufacturer's protocol. ATP production was inhibited by incubation of MA-10 cells with various concentrations of carbonyl cyanide m-chlorophenyl hydrazone (mCCCP) for 1 h as described previously (Prasad et al., 2017).

Metabolic conversion/Activity assays

To measure the conversion of cholesterol to pregnenolone, isolated mitochondria were incubated with 80,000 counts of ^{14}C-cholesterol (PerkinElmer, Whatman, MA). Reactions were initiated by addition of 50μM NADPH (Sigma-Aldrich) and incubated at 37°C for 2 h in a shaking water bath. For conversion of progesterone analysis the reactions were performed with NADH following our published procedure (Pawlak et al., 2011b; Prasad et al., 2016). To stop pregnenolone to progesterone conversion, we have incubated with 3-beta Hydroxy steroid dehydrogenase inhibitor (3βHSD2) with 10 pmol of Trilostane (Tril) (Prasad et al., 2012). For digitonin solubilized complex activity was performed after isolation of the complex in presence and absence of digitonin and performed the conversion with NADH following the

same procedure. Steroids were extracted following our previous procedure (Pawlak et al., 2011b; Prasad et al., 2017; Prasad et al., 2016) and the amounts of steroid were determined by using a phosphorimager.

Calorimetry

Mitochondria were prepared as described previously and for the specific experiment 0.1 mg of mitochondrial protein was suspended in 1.5 mL of buffer (Bose et al., 2002). The solution was titrated with mitochondria, succinate and ATP in a MicroCal (Northampton, MA) VP-ITC calorimeter equipped with an automatic injector in the Department of Biochemistry and Molecular Biology at the University of Florida, Gainesville. All buffers were filtered through 0.22 μm and degassed before use. Data were collected by incubating mitochondria in the cell for 2 h prior to the injection of succinate or cholesterol in 5 μL at a speed of 0.5 μL/s with a gap of 7 min for each injection for equilibration. Enthalpy (ΔH) was measured by integration of excess power generated by the reaction divided by the concentration of the injectant.

Transmission electron microscopy (TEM)

To determine the precise localization of SCC in mice testis mitochondria, TEM experiments were carried out. Testes tissue was fixed overnight in 4% formaldehyde and 0.2% glutaraldehyde in 0.1M sodium cacodylate buffer, pH 7.4. Tissues were dehydrated through a graded ethanol series from 25% to 95% and embedded in LR white resin. Sectioning was performed on a Leica EM UC6 ultramicrotome (Leica Microsystems, Bannockburn, IL), and 75nm-thick sections were collected on 200 mesh nickel grids. Sections were etched with 2% H_2O_2, quenched in 1M NH_4CL, and blocked in 0.1% BSA in PBS for 4 h at room temperature in a humidified atmosphere, followed by incubation with anti-SCC (1:1000 dilution) in 0.1% BSA overnight at 4°C. Sections were washed in PBS (5 times) and floated on drops of anti-primary-specific, ultra-small (<1.0 nm) NanogoldTM reagent (Nanoprobes, Yaphank, NY) diluted 1:2000 in 0.1% BSA in PBS at room temperature for 2-4 h. Sections were washed with PBS (5 times, 10 min each) and deionized H_2O (5 times, 10 min each), prior to enhancement with HQ SilverTM (Nanoprobes) for 8 min. Enhancement was terminated by washing in cold deionized H_2O. For double

antibody immunolabeling, sections were labeled with anti-SCC (1:1000) overnight at 4°C, followed by incubation with anti-Calnexin (1:2000) overnight at 4°C. Silver enhancement of anti-SCC nanogold was twice the duration of anti-Calnexin nanogold. Thus, two different sizes of gold particles were obtained. Sections were then stained with 2% uranyl acetate in 70% ethanol, washed with deionized H_2O (5 times, 2 min each), and air dried. Average size of large gold particles was 55 nm in diameter with 90% being between 45-65 nm in diameter. Average size of small gold particles was 15 nm in diameter with 90% of the gold particles being <25 nm in diameter. Tissue sections were imaged using a JEM 1230 transmission electron microscope (JEOL Peabody, MA) at 110 kV and an UltraScan 4000 CCD camera and first Light Digital Camera Controller (Gatan Inc., Pleasanton, CA). Approximately 80 sections from each experiment were analyzed.

Figure preparation and data analysis

The images were obtained from the autoradiographic films or scanning through a phosphorimager, and the data analysis was performed using, Kalidagraph, or Microsoft Excel.

Supplementary Figure Legend

Figure S1 (Related to Figure 1, panels E-H). Enlarged EM of the mouse testis stained with SCC antibody. The distance of mitochondria from the ER is shown in blue arrow.

Figure S2 (Related to Figure 1, panels K-M). Analysis SCC processing. (A), Overexpression of SCC in COS-1 cells at the indicated time detected by Western blotting with a SCC antibody. The red arrow head shows the minimum start of expression and blue arrow head shows start of major conversion from 61 kDa to 51 kDa. Bottom, Western blot of the same fractions from Panel A with VDAC2 antibody. (B), Density gradient separation of the digitonin solubilized mouse mitochondrial tissue through sucrose density gradient centrifugation and visualized by Western blotting with a SCC antibody. Appearance of 57-kDa and 51-kDa SCC is indicated with black and red arrow. Bottom, The top membrane with longer exposure. (C), Western staining of the same digitonin lysate fractions with a VDAC2 antibody.

Figure S3 (Related to Figure 3). Difference in activity with pre and post incubation with succinate. (A), Thin layer chromatography showing the metabolic conversion pattern. (B), Analysis of the role of succinate due to pre and post incubation shown in a flow chart.

Figure S4 (Related to Figure 4). Metabolic activity determination. (A), Measurement of activity (^{14}C-cholesterol to pregnenolone conversion) with mitochondria isolated from MA-10 cells over different periods of time from 5 min to 2 hour. (B), Measurement of activity (^{3}H-pregnenolone to progesterone conversion) with mitochondria isolated from MA-10 cells as well as the digitonin lysate of the MA-10 mitochondria prepared in presence and absence of succinate. Trilostane (Tril) was added to inhibit 3βHSD2 activity to stop conversion after pregnenolone synthesis.

Figure S5 (Related to Figure 5). Expression analysis of the malate dehydrogenase. Top, Western blot analysis of malate dehydrogenase knock down stable clones 1 and 2, and its comparison with MA-10 cells with MDH2 antibody. Bottom, Western of the clones 1 and 2 from the top panel with pyruvate dehydrogenase (PDC-E2) antibody.

SUPPLEMENTAL REFERENCES

Bose, H.S., Gebrail, F., Marshall, B., Perry, E.W., and Whittal, R.W. (2019). Inner mitochondrial translocase Tim 50 is central in adrenal and testicular steroid synthesis. Mol Cell Biol *39*, doi:10.1128/MCB.00484-00418.

Bose, H.S., Lingappa, V.R., and Miller, W.L. (2002). Rapid regulation of steroidogenesis by mitochondrial protein import. Nature *417*, 87-91.

Bose, M., Whittal, R.M., Miller, W.L., and Bose, H.S. (2008). Steroidogenic activity of StAR requires contact with mitochondrial VDAC1 and phosphate carrier protein. J Biol Chem *283*, 8837-8845.

Marriott, K.C., Prasad, M., Thapliyal, V., and Bose, H.S. (2012). Sigma-1 receptor at the mitochondrial associated ER-membrane is responsible for mitochondrial metabolic regulation. J Pharmacol Exp Ther *343*, 578-586.

Pawlak, K.J., Prasad, M., McKenzie, K.A., Wiebe, J.P., Gairola, C.G., Whittal, R.M., and Bose, H.S. (2011a). Decreased cytochrome c oxidase IV expression reduces steroidogenesis. J Pharmacol Exp Ther *338*, 598-604.

Pawlak, K.J., Prasad, M., Thomas, J.L., Whittal, R.M., and Bose, H.S. (2011b). Inner mitochondrial translocase Tim50 interacts with 3beta-hydroxysteroid dehydrogenase type-2 to regulate adrenal and gonadal steroidogenesis. J Biol Chem *286*, 39130-39140

Prasad, M., Pawlak, K.J., Burak, W.E., Perry, E.E., Marshall, B., Whittal, R.M., and Bose, H.S. (2017). Mitochondrial metabolic regulation by GRP78. Science Advances *3*, e1602038.

Prasad, M., Thomas, J.L., Whittal, R.M., and Bose, H.S. (2012). Mitochondrial 3-beta hydroxysteroid dehydrogenase enzyme activity requires a reversible pH-dependent conformational change at the intermembrane space J Biol Chem *287*, 9534-9546.

Prasad, M., Walker, A.N., Kaur, J., Thomas, J.L., Powell, S.A., Pandey, A.V., Whittal, R.M., Burak, W.E., Petruzzelli, G., and Bose, H.S. (2016). Endoplasmic reticulum stress enhances

mitochondrial metabolic activity in mammalian adrenals and gonads. Mol Cell Biol *36*, 3058-3074.

Ragan, C.I., Wlson, M.T., Darley-Usmer, V.M., and Lowe, P.N. (1986). Sub-Fractionation of mitochondria and isolation of the proteins of oxidative phosphorylation (Washington, D.C.: IRL Press).

SUPPLEMENTAL FIGURES

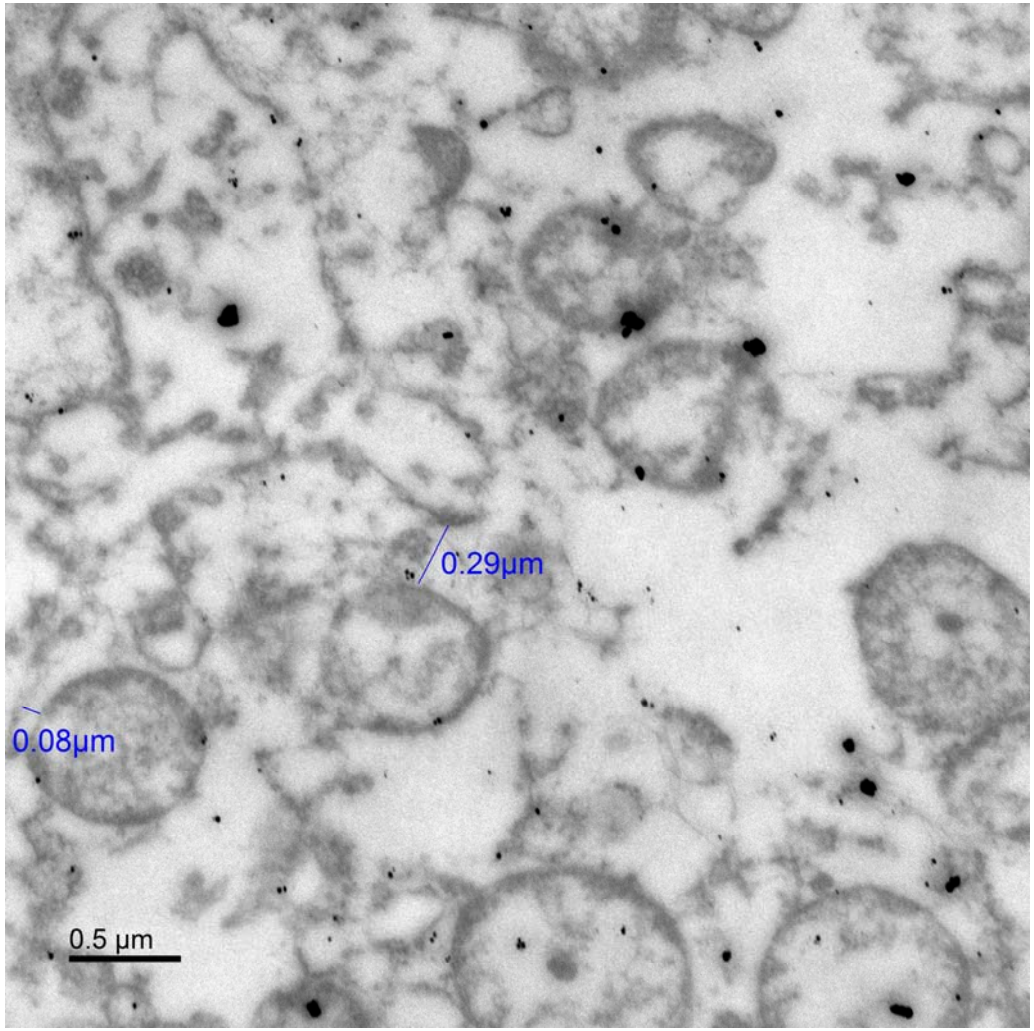

FIGURE S1

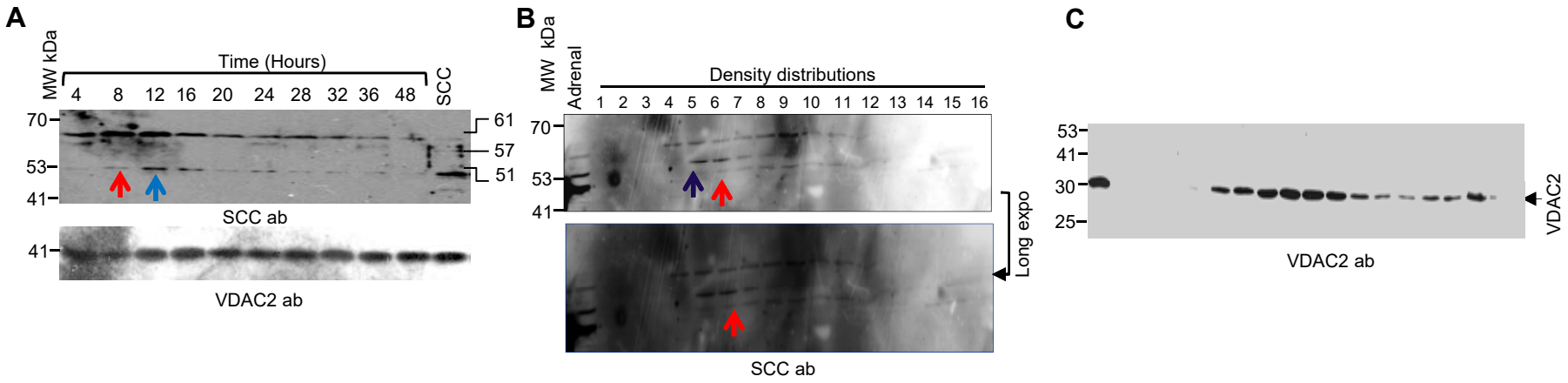
A
MW kDa
Time (Hours)
4 8 12 16 20 24 28 32 36 48 SCC
70
53
41
61
57
51
SCC ab
41
VDAC2 ab
B
MW kDa
Adrenal
Density distributions
1 2 3 4 5 6 7 8 9 10 11 12 13 14 15 16
70
53
41
Long expo
SCC ab
C
53
41
30
25
VDAC2
VDAC2 ab

FIGURE S2

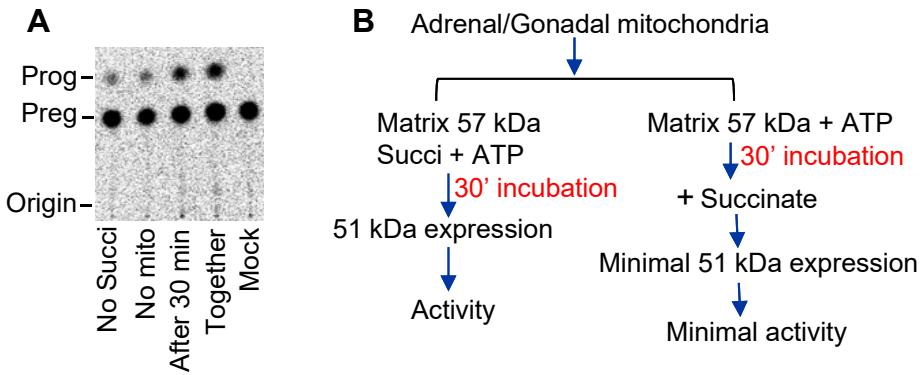
A
Prog
Preg
Origin
No Succi
No mito
After 30 min
Together
Mock
B
Adrenal/Gonadal mitochondria
Matrix 57 kDa
Succi + ATP
30' incubation
51 kDa expression
Activity
Matrix 57 kDa + ATP
30' incubation
+ Succinate
Minimal 51 kDa expression
Minimal activity

FIGURE S3

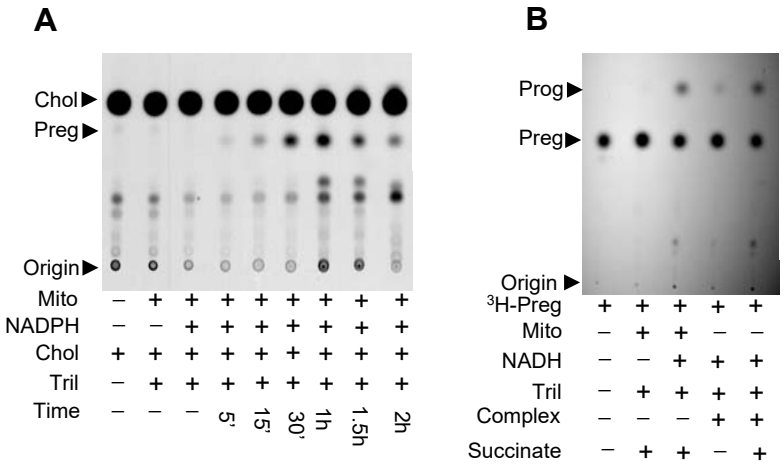
A
Chol
Preg
Origin
Mito – + + + + + + + +
NADPH – – + + + + + + +
Chol + + + + + + + + +
Tril – + + + + + + + +
Time – – – 5' 15' 30' 1h 1.5h 2h
B
Prog
Preg
Origin
3H-Preg + + + + +
Mito – + + – –
NADH – – + + +
Tril – + + + +
Complex – – – + +
Succinate – + + – +

FIGURE S4

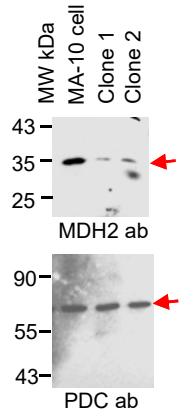

FIGURE S5